1

2

Transmigration of *Trypanosoma cruzi* trypomastigotes through 3D cultures resembling a physiological environment

5

Matías Exequiel Rodríguez[1], Mariana Rizzi[1], Lucas D. Caeiro[1], Yamil E. Masip[1], Alina Perrone[2], Daniel O. Sánchez[1], Jacqueline Búa[2], Valeria Tekiel[1]*

9

[1]Instituto de Investigaciones Biotecnológicas "Dr. R. Ugalde" (IIBIO) Universidad Nacional de San Martín (UNSAM) - CONICET, San Martín, Provincia de Buenos Aires, Argentina.

[2]Instituto Nacional de Parasitología 'Dr Mario Fatala Chaben', ANLIS CG Malbrán. Buenos Aires, Argentina.

15

* Corresponding author

E-mail: valet@iib.unsam.edu.ar; vtekiel@gmail.com

18

19

1

Abstract

Chagas´disease, caused by the kinetoplastid parasite *Trypanosoma cruzi*, presents a variety of chronic clinical manifestations whose determinants are still unknown but probably influenced by the host-parasite interplay established during the first stages of the infection, when bloodstream circulating trypomastigotes disseminate to different organs and tissues. After leaving the blood, trypomastigotes must migrate through tissues to invade cells and establish a chronic infection. How this process occurs remains unexplored. Three-dimensional (3D) cultures are physiologically relevant because mimic the microarchitecture of tissues and provide an environment similar to the encountered in natural infections. In this work, we combined the 3D culture technology with host-pathogen interaction, by studying transmigration of trypomastigotes into 3D spheroids. *T. cruzi* strains with similar infection dynamics in 2D monolayer cultures but with different *in vivo* behavior (CL Brener, virulent; SylvioX10 no virulent) presented different infection rates in spheroids (CL Brener ~40%, SylvioX10 <10%). Confocal microscopy images evidenced that trypomastigotes from CL Brener and other highly virulent strains presented a great ability to transmigrate inside 3D spheroids: as soon as 4 hours post infection parasites were found at 50 µm in depth inside the spheroids. CL Brener trypomastigotes were evenly distributed and systematically observed in the space between cells, suggesting a paracellular route of transmigration to deepen into the spheroids. On the other hand, poor virulent strains presented a weak migratory capacity and remained in the external layers of spheroids (<10µm) with a patch-like distribution pattern. The invasiveness -understood as the ability to transmigrate deep into spheroids- was not a transferable feature

2

45 between strains, neither by soluble or secreted factors nor by co-cultivation of

46 trypomastigotes from invasive and non-invasive strains. We also studied the

47 transmigration of recent *T. cruzi* isolates from children that were born

48 congenitally infected, which showed a high migrant phenotype while an isolate

49 form an infected mother (that never transmitted the infection to any of her 3

50 children) was significantly less migratory. Altogether, our results demonstrate

51 that in a 3D microenvironment each strain presents a characteristic migration

52 pattern and distribution of parasites in the spheroids that can be associated to

53 their *in vivo* behavior. Certainly, the findings presented here could not have been

54 studied with traditional 2D monolayer cultures.

55

Author Summary

56

57 *Trypanosoma cruzi* is the protozoan parasite that causes Chagas´ disease, also

58 known as American trypanosomiasis. Experimental models of the infection

59 evidence that different strains of the parasite present different virulence in the

60 host, which cannot be always reproduced in 2D monolayer cultures. Three

61 dimensional (3D) cultures can be useful models to study complex host-parasite

62 interactions because they mimic *in vitro* the microarchitecture of tissues and

63 provide an environment similar to the encountered in natural infections. In

64 particular, spheroids are small 3D aggregates of cells that interact with each

65 other and with the extracellular matrix that they secrete resembling the original

66 microenvironment both functionally and structurally. Spheroids have rarely been

67 employed to explore infectious diseases and host-parasite interactions. In this

68 work we studied how bloodstream trypomastigotes transmigrate through 3D

3

69   spheroids mimicking the picture encountered by parasites in tissues soon after

70   leaving circulation. We showed that the behavior of *T. cruzi* trypomastigotes in

71   3D cultures reflects their *in vivo* virulence: virulent strains transmigrate deeply

72   into spheroids while non-virulent strains remain in the external layers of

73   spheroids. Besides, this work demonstrates the usefulness of 3D cultures as an

74   accurate *in vitro* model for the study of host-pathogen interactions that could not

75   be addressed with conventional monolayer cultures.

76

Introduction

78   The protozoan parasite *Trypanosoma cruzi* is the etiological agent of Chagas

79   disease, which currently affects about 8 million people. Chagas' disease is an

80   endemic illness in Latin America that has spread worldwide in the past years.

81   The infection usually develops as a chronic cardiac, digestive or neurologic

82   pathology. The reason why symptoms appear 10 or more years after the initial

83   infection, and only in ~40% of individuals, remains unsolved, but both host and

84   parasite genetic background should have an impact on the disease outcome.

85   Chagas disease is one of the main health problems in Latin America, causing

86   more than 10000 deaths per year, and incapacity in infected individuals [1].

87   In humans, the infection initiates with trypomastigotes deposited on

88   mucous or skin, along with triatomine bug faeces, when the insect vector feeds

89   on blood. Trypomastigotes are able to invade any nucleate cells at the infection

90   site. Once inside the cell, trypomastigotes differentiate to amastigotes, which are

91   the intracellular and replicative form. After several division cycles, amastigotes

92   differentiate again into trypomastigotes, the infected cells burst, and parasites

4

93   are released into the interstitial space. Trypomastigotes can either infect

94   neighboring cells or spread distantly by circulation. Successive cycles of

95   intracellular infection and replication followed by bloodstream trypomastigote

96   dissemination are the hallmark of the initial acute phase, which drives the

97   amplification of the parasitic load, and eventually produces the infection of

98   organs and tissues [2]. The acute phase ends approximately 2-3 months after

99   the initial infection, the time required by the host immune system to control

100   parasitemia and clear most trypomastigotes from peripheral circulation.

101   However, a chronic and persistent infection is already established, characterized

102   by the presence of intracellular amastigotes essentially confined into tissues

103   along with positive serologic tests [2,3].

104   The experimental murine model allowed to understand that during the

105   acute phase, trypomastigotes disseminate from the inoculation site to almost all

106   tissues, to render completely parasitized mice, few days after the initial infection

107   [4]. This entails that trypomastigotes should be able to escape from peripheral

108   circulation, cross the vascular endothelium and migrate through the extracellular

109   matrix (ECM) to establish a tisular intracellular infection [5]. The effectiveness of

110   trypomastigotes to cross biological barriers and migrate through tissues will

111   impact on *T. cruzi* ability to produce a severe, moderate or mild tissue infection.

112   This process -that can be linked to parasite virulence and dynamic of infection *in*

113   *vivo*- is poorly understood. Some authors suggested that the rupture of the

114   endothelial barrier is necessary for the infection of target tissues [6]. On the

115   contrary, others showed that trypomastigotes traverse the endothelial barrier

116   involving a transcellular traffic of trypomastigotes through endothelial cells,

117   mediated by the activation of the bradykinin receptor 2, and without disturbing its

118 integrity nor its permeability [7]. Since different combinations of parasite and

119 mouse strains present differential tissue colonization and target organs of

120 damage [8,9], the differences between both proposed transmigration models

121 could be attributed to the different strains employed. Either way, trypomastigote

122 transmigration through tissues is an essential event for *T. cruzi* infection. Studies

123 on *T. cruzi* transmigration have been very limited, probably because of the

124 extremely simplicity of monolayers cultures and –on the other hand- the

125 complexity of *in vivo* models, which present low spatio-temporal resolution.

126 Three-dimensional (3D) cultures are physiologically relevant and a good

127 alternative because they mimic the microarchitecture of tissues and can provide

128 an environment similar to the encountered in natural infections [10].

129 Spheroids are small aggregates of cells that do not adhere to a culture

130 substrate and grow in 3D. Cells interact with each other and secrete the

131 extracellular matrix (ECM) in which they reside, resembling their original

132 microenvironment both functionally and structurally [11,12]. Spheroids have

133 been broadly employed and deeply contribute to understand mechanisms in

134 cancer biology and immunology [13-15], but they have rarely been employed to

135 explore infectious diseases and host-parasite interactions. Remarkably, the co-

136 culture of spheroids of myocytes with *T. cruzi* trypomastigotes has demonstrated

137 to be an accurate model of fibrosis and hypertrophy that adequately recreates

138 the chronic chagasic cardiomyopathy [16,17]. In the present work we took

139 advantage of the 3D spheroid technology to disclose how trypomastigotes

140 transmigrate across tissues, which is a key process of the host-parasite interplay

141 in the early steps of infection. We demonstrate that the invasiveness of

6

142 trypomastigotes from different *T. cruzi* strains and isolates into spheroids can be

143 associated with their *in vivo* behavior and virulence.

144

Materials and Methods

Reagents and sera

147 Ultrapure Agarose, Carboxy-fluoresceinsuccinimidyl ester (CFSE) and

148 CellTraceTM Far Red (CTFR) were acquired from Invitrogen. Polyethylenimine

149 (PolyAr87-PEI) transfection reagent was obtained from FFyB (University of

150 Buenos Aires). Anti *T. cruzi* antisera developed in mice was generated in our

151 laboratory and used along with goat anti-mouse conjugated to Alexa-488 or

152 Alexa-647 (Molecular Probes).

Parasites and conditioned media

154 *T. cruzi* trypomastigotes from different strains and DTUs employed were:

155 SylvioX10, K98, Dm28, 193-733MM and 199-173BB (DTU TcI); Y (DTU TcII);

156 185-748BB and 186-401BB (DTU TcV) and RA and CL Brener (DTU TcVI). All

157 strains were DNA genotyped by PCR-RFLP of *TcSC5D* and *TcMK* genes (S1

158 Fig), as described [18].

159 Parasites were routinely maintained by *in vitro* cultures on Vero cells as

160 previously described [19], and trypomastigotes harvested from supernatants.

161 Culture-derived trypomastigotes were labeled with CellTrace™ CFSE as we

162 previously described [20]. Trypomastigotes were alternatively labelled with

163 CellTrace™ Far Red CTFR (5 µM), essentially with the same protocol with slight

7

164   differences in the incubation time (20 min at 37ºC, followed by the addition of 1

165   ml of complete medium and an additional incubation of 5 min at 37°C in the

166   dark). After labelling, the motility of parasites was controlled under light

167   microscope. The percentage of labelled parasites and the fluorescence intensity

168   of CFSE and CTFR was determined by flow cytometry.

169   *T. cruzi* derived conditioned medium (CM) was obtained by a previously

170   standardized protocol [21]. In brief, cell-derived trypomastigotes (100×10^6) were

171   washed with PBS, resuspended in 1 ml of MEM without serum (or MEM without

172   parasites as control medium) and incubated for 6 h at 37°C in a 5% CO_2

173   humidified atmosphere. Then, parasites were pelleted by centrifugation and the

174   cell-free supernatant (containing both extracellular vesicles as well as vesicle-

175   free secreted material) was centrifuged twice for 10 min at 15000 xg. The

176   clarified supernatant was filtered through a 0.45 µm syringe filter, to obtain the

177   CM, which was aliquoted and stored at -70°C until use.

178   **Cell culture and stable HeLaR2 cell line generation**

179   Vero, HeLa and HEK293T cells were grown in MEM (Gibco) supplemented with

180   10% (v/v) fetal bovine serum (Natocor), 100 U/ml penicillin and 10 µg/ml

181   streptomycin. Cells were maintained at 37°C in 5% CO_2 and 95% air in a

182   humidified incubator. To obtain Hela cells stably expressing LifeAct-RFP,

183   permissive HEK293T cells were first employed to produce lentiviral particles

184   packed with LifeAct-RFP, essentially as described by Gerber *et al* [22]. Briefly,

185   HEK293T were seeded on 24-well plates (3×10^4 cells/well) and transfected 24 h

186   later by the PEI method with a mix of 0.5 µg pCMV-dR8.9 DVpr (packaging

187   plasmid), 0.05 µg pCMV–VSV-G (envelope plasmid) and 0.5 µg of the pLenti

8

LifeAct-RFP (transfer plasmid) per well. The supernatant containing lentiviral particles packed with LifeAct-RFP was collected at 48 and 72 h after transfection, precleared, and concentrated by centrifugation. HeLa cells (3×10^4 cells/well) were transduced in MEM containing 10% FBS with a 0.3 m.o.i. of lentiviral particles, and expanded in culture flasks. Cells expressing LifeAct-RFP (HeLaR) were sorted by flow cytometry, and cloned by limiting dilution. The clone number 2 (HeLaR2) stably expressing LifeAct-RFP was selected and employed for all the experiments.

HeLa spheroids and infection model

Spheroids of HeLaR2 cells were generated by the liquid overlay method [23]. Cells (1000/well) were added to U-bottom 96-well plates coated with agarose 1% in PBS (w/v) and cultured in MEM 10% FBS. The formation of spheroids was controlled by microscopy from 24 h post seeding (S2 Fig). At 72 h, each well contained one spheroid of 300-400 μm diameter, conformed by ≃9000 cells.

For *T. cruzi* infection, twelve spheroids were placed on each well of an agarose pre-coated p24 plate and incubated with 1 or 10 m.o.i. of trypomastigotes (or control medium) for 1 or 24 h, in MEM supplemented with 4% FBS. When appropriate, 100 μl of medium was replaced by 100 μl of CM. When indicated, 2D-monolayers of HeLaR2 cells (10×10^5 cells/well) were incubated with 1 or 10 m.o.i. of trypomastigotes also labelled with CFSE in a final volume of 500 μl of MEM 4%.

9

209 For co-infection assays, 12 spheroids (in one p24 well) were simultaneously

210 incubated with CL Brener and SylvioX10 for 24 h with 10 m.o.i. of each *T. cruzi*

211 strain, labelled with a different stain.

212 **Cellular infection determined by flow cytometry**

213 Infected spheroids were collected in 1.5 ml tubes, washed three times with PBS

214 and disaggregated by addition of 200 µl 0,25% trypsin/EDTA for 10 min at 37ºC.

215 The cellular pellet -collected by centrifugation 10 min at 1000 x g- was washed

216 three times and fixed in PBS 0.5% PFA. Infected 2D-monolayer cells were

217 trypsinized and treated like 3D spheroids. Samples were acquired on a

218 FACSCalibur (Becton Dickinson); gated HeLaR2 by forward and side scatter

219 parameters were selected. A total of 10,000 events were analyzed for each

220 condition. FL1- cells represented uninfected HeLaR2 cells while FL1+

221 represented cells infected (either with intracellular parasites and/or attached to

222 cell membrane) with CFSE-labelled parasites, FL4+ cells were those infected

223 with CTFR-labelled parasites. Data was analyzed using FlowJo v10.0.7

224 software. Statistical significance was determined by two-tailed unpaired student *t*

225 *test* (Prism, GraphPad Software).

226 **Quantification of free-parasites inside spheroids**

227 Infected spheroids disaggregated by trypsin treatment were centrifuged for 10

228 min at 5700 x g to collect HeLaR2 cells and parasites that were infecting or

229 attached to HeLa cells, as well as parasites that were free inside spheroids (i.e.

230 not associated to cells but inside spheroids). The pellet was then analysed by

231 confocal microscopy to determine infected cells as well as free parasites

232 (expressed as number of free-parasites for each 100 HeLaR2 cells). Statistical

10

233 significance was determined by two-tailed unpaired student *t test* (Prism,

234 GraphPad Software).

Parasitic load into spheroids

236 The total cargo of parasites inside the spheroids, either infecting cells or free in

237 the ECM, was determined by qPCR. For doing so, each treatment was carried

238 out by duplicate: one sample was used to determine the parasite load

239 associated to spheroids (sample 1) while the other was used to determine the

240 total cargo of parasites in the well (sample 2: parasites associated to spheroids

241 plus parasites free in the medium/well). Infection was carried out as mentioned

242 above. After 24 h, spheroids from sample 1 were collected in 1,5 ml tubes and

243 carefully washed five times with sterile PBS to eliminate parasites from the

244 supernatant avoiding the disassembling of spheroids. Instead, for sample 2

245 spheroids and medium were collected together, centrifuged for 10 min at 5700 x

246 g and the pellet washed with sterile PBS. Samples were subjected to a standard

247 salting out protocol to obtain genomic DNA [24]. gDNA concentration was

248 measured using Nanodrop and 50 ng were used in each qPCR reaction, which

249 were carried out with Kapa Sybr Fast Universal Kit (Biosystems) in a 7500 Real

250 Time PCR System (Applied Biosystems). The *T. cruzi* single copy gene *PCD6*

251 (TcCLB.507099.50) was amplified with primers v099.50bFw

252 (CAGGCATCACCGTATTTTCCA) and 099.50bRev

253 (CTCTTGTTCCGTGCCAAACA) [25]. To determine *T. cruzi* DNA (*Tc*DNA)

254 abundance, DNA content was normalized to human *GAPDH* gene (53MFZ-

255 GAPDHFw: ACCACCCTGTTGCTGTAGCCAAAT and 54MFZ-Rev:

256 GACCTGACCTGCCGTCTAGAAAAA). Results were analysed with the LinReg

11

257 software [26]. The percentage of *Tc*DNA inside spheroids was calculated as

258 X%= *Tc*DNA$_{sample1}$ x 100 / *Tc*DNA$_{sample2}$ and expressed as mean ± SD of three

259 independent experiments. Statistical significance was determined by student *t*

260 *test* (GraphPad software).

261 **Parasite invasiveness and dissemination**

262 Infected spheroids were fixed by adding PFA to a 3.2% final concentration and

263 incubated at 37°C for 1.5 h. Then, spheroids were washed with PBS as

264 described previously [20] and mounted. Fluorescence images were acquired

265 with a confocal Olympus FV1000 microscope. CFSE or CTFR labelled parasites

266 were imaged with a 488 nm or 647 nm laser, respectively, while HeLaR2 cells

267 were imaged at 530 nm. Z-stacks were collected with a 10x objective from 0 to

268 150 μm in depth with 2 μm intervals in the vertical z-axis. Alternatively, images

269 were acquired with a 40x objective, and the spheroid was scanned at 10, 30 and

270 50 μm in depth from the surface. To determine the localization of parasites,

271 spheroids were analyzed with a 60x objective and Z-stacks were collected at 0.2

272 μm intervals in the z-axis. All images were analyzed with ImageJ [27] software;

273 3D reconstructions and 3D-movies were generated with the 3D-viewer plugin.

274 **Electron microscopy**

275 Infected spheroids were fixed in 4% PFA and serially dehydrated with increasing

276 ethanol solutions (10-100 %) followed by critical point drying with carbon dioxide.

277 Samples were then coated with 60%/40% palladium/gold and acquired with a

278 scanning electron microscope (Philips - XL Serie 30).

279

280 **Free-swimming assay**

12

281   Trypomastigotes (15×10^6) were resuspended in 5 ml MEM 4% SFB, transferred

282   to round-bottom centrifuge tubes (Oak Ridge Style) and centrifuged at 2,500 x g

283   for 8 min, which resulted in parasites at the bottom of the tubes forming a thin

284   pellet. The tubes were then incubated 2 h at 37°C, to allow trypomastigotes to

285   freely swim. Aliquots of 1 ml were carefully taken from the top (layer 5) to the

286   bottom; the pellet was resuspended in 1 ml of medium. Parasites in each fraction

287   were enumerated by counting in a Neubauer chamber.

288   **Statistical analysis**

289   All statistical analyses and graphs were performed with GraphPad Prism 7

290   (GraphPad Software, USA). We used a two-tailed unpaired *t test* when the

291   means of two groups were compared. When more than 2 groups were

292   compared, we used two-way ANOVA with Bonferroni multiple comparison test.

293   Significant differences were designed when P-value (P) n.s. ≥ 0.05, *p<0.05,

294   **p<0.01, ***p<0.001.

295

296   **Results**

297   ***T. cruzi* trypomastigotes are less infective in 3D spheroids than in 2D**

298   **monolayer cultures.**

299   *Trypanosoma cruzi* presents a high genetic heterogeneity and, currently,

300   *T. cruzi* strains are classified into six clusters or discrete typing units (DTUs),

301   named TcI to TcVI [28]. We selected CL Brener (DTU TcVI) and SylvioX10 (DTU

302   TcI) strains, of high and low virulence, respectively, and whose biologically

303   distinctive behavior in experimental models of *T. cruzi* infection is well

13

304   characterized [8,29-31].

305   HeLa cells constitutively expressing LifeAct-RFP (HelaR2 hereon), along

306   with trypomastigotes labelled with CFSE or CTFR were employed to monitor

307   short-time infection dynamics and host-parasite interactions (Fig 1). We first

308   evaluated the infection profile of trypomastigotes both on conventional 2D

309   monolayers and in 3D spheroids (Fig 2). While on conventional 2D monolayer

310   cultures CL Brener and SylvioX10 parasites showed similar infection rates

311   (~70%) (Fig 2A,C), both strains were much less effective to infect 3D spheroids

312   (Fig 2B,C) and with differences between both strains. Infection with CL Brener

313   rendered higher number of cells with cell-attached or internalized parasites

314   (38,2% CL Brener vs 8,5% SylvioX10), as detected by flow cytometry of

315   disaggregated spheroids (Fig 2B). The total cargo of parasites inside the

316   spheroids, which includes intracellular parasites, surface attached, as well as

317   free parasites migrating inside spheroids through the extracellular matrix, was

318   also higher on CL Brener than SylvioX10 infected spheroids (48% *vs* 18%,

319   determined by qPCR; Fig 2D). Differences between strains were also registered

320   when free-parasites (i.e. not associated to cells) inside spheroids were

321   enumerated (Fig 2E-F). Altogether, these results evidence that both strains have

322   different abilities to infect 3D cultures, being CL Brener strain 2-3 fold more

323   infectious than SylvioX10. These findings were also registered with different

324   multiplicity of infection, and contrast with the similar behavior of both strains on

325   monolayer cultures (S3 Fig).

326   **Trypomastigotes from different strains disseminate differentially inside**

327   **spheroids.**

14

328   A panoramic view of spheroids, reconstructed from confocal stacks shows that

329   SylvioX10 trypomastigotes were preferentially localized at the spheroid surface.

330   Parasites were mostly focalized in large clumps that resembled a "patch-like"

331   distribution pattern (Fig 3A**,** S1 movie). By contrast, CL Brener parasites were

332   evenly distributed all over the surface of spheroids (Fig 3B, S2 movie).

333   The transmigration and invasiveness of trypomastigotes was analyzed by

334   scanning the spheroids by confocal microscopy. Most SylvioX10 trypomastigotes

335   were retained at spheroid surface or at the first layers of cells, and only scarce

336   trypomastigotes were detected up to 30 μm in depth (Fig 3C). On the other

337   hand, CL Brener parasites were able to deepen into spheroids: migrated

338   uniformly and were easily detected up to 50 μm in depth (Fig 3D). The migration

339   through the spheroid seems to be a fast movement because similar patterns

340   were observed from 1 h post infection (S4 Fig). In brief, confocal scanning

341   evidenced that CL Brener trypomastigotes can efficiently transmigrate deeply

342   into spheroids, while SylvioX10 is retained at the surface, which corresponds

343   with the differential virulence of both strains.

344   **Trypomastigotes of high migratory CL Brener strain use a paracellular**

345   **migration route to move inside spheroids.**

346   To answer how trypomastigotes spread within spheroids, we analyzed the

347   parasite-spheroid interaction with higher resolution techniques, such as scanning

348   electron microscopy (SEM) and higher power snapshots by confocal

349   microscopy.

350   As evidenced by confocal microscopy, SEM images also showed numerous

351   SylvioX10 parasites attached to the surface of individual cells (Fig 4A, panels b,

15

352 c; white arrows). Notably, CL Brener trypomastigotes were predominantly caught

353 entering into spheroids through the space between cell-cell junctions (Fig 4A**,**

354 panels e, f; white asterisks). Spheroids infected with SylvioX10 also presented

355 multiple intracellular amastigotes in the superficial layers -first 10 µm- of cells

356 with an untidy distribution (Fig 4B panels a, b and c; 4C and S3 movie)**.**

357 Confocal slices of spheroids infected with CL Brener made evident that there is

358 an orderly distribution pattern around cell-cell contacts (Fig 4B panels d, e, f;

359 white asterisks). At shorter times, CL Brener trypomastigotes were plainly

360 observed in the space between cells, on their way through the extracellular

361 matrix, suggesting a paracellular route of transmigration within the spheroid (Fig

362 4D and S4 and S5 movies). CL Brener trypomastigotes were also detected

363 intracellularly, though fastened to the cellular membrane (S6 movie).

364 **The capacity of transmigration is not transferable between strains.**

365 CL Brener and SylvioX10 strains presented not only dissimilar invasiveness

366 profiles, but also their allocation at the superficial layers of spheroids was very

367 distinctive (Fig 3 and 4). We then investigated if transmigration could be

368 transferred from the highly migrant CL Brener strain to the low migrant

369 SylvioX10, through soluble or secreted factors or by co-cultivation of both strains

370 (Fig 5). Interestingly, each strain retained its own dissemination pattern (Fig 5A)

371 and rate of infection (Fig 5B) irrespective of the presence (or absence) of the

372 other strain. Conditioned media (including both soluble and vesicle-contained

373 secreted factors) from CL Brener or SylvioX10 did not cause changes in the

374 invasiveness pattern or percentage of infected cells (S5 Fig). Together, these

375 results indicate that the transmigration capacity of *T. cruzi* is a strain-specific trait

376 that cannot be transferable by soluble or secreted factors, nor through co-

16

377   cultivation of migrant and non-migrant trypomastigotes.

378   **Transmigration deep inside spheroids can be linked to virulence.**

379   To evaluate if the differential transmigration profile could be linked to parasite

380   DTU or virulence, the transmigration into spheroids of other well characterized *T.*

381   *cruzi* strains was also analyzed. Low virulent strains (K98 and Dm28; TcI)

382   presented low ability to transmigrate into spheroids (Fig 6). In contrast, virulent

383   strains (RA [TcVI] and Y [TcII]) showed a transmigration pattern resembling the

384   observed for CL Brener (Fig 6) (Fig 6A and S7 and 8 movies).

385   Finally, we analyzed the transmigration of four recent clinical isolates of *T. cruzi*.

386   One isolate was derived from a *T. cruzi*-infected mother that after several

387   pregnancies never delivered an infected child (isolate 773MM, TcI; non-

388   congenital transmission). The other isolates, derived from babies that were born

389   congenitally infected (isolates 173BB, TcI; 748BB, TcV; and 401BB, TcV;

390   congenital transmission) [32]. The non-congenital isolate (733MM) [32] showed

391   a low ability to migrate deep inside spheroids. Also, a "patch-like' distribution

392   pattern, similar to the observed with SylvioX10 strain was observed (Fig 7B). In

393   contrast, congenitally isolated parasites presented a highly migrant phenotype.

394   Either DTU TcI or TcV isolates from congenitally infected babies were found

395   deeply inside spheroids and easily visualized along the first 50 μm in depth (Fig

396   7A).

397   The cellular infection produced by 733MM was ~20%, a value near the one

398   registered with the low virulent SylvioX10 strain, while the 40% of infection of

399   cells in spheroids produced by congenital isolates resembled the infection

400   produced by CL Brener strain (Fig 7C).

17

401 Ultimately, because trypomastigotes of different strains behave differently when

402 they are allowed to swim freely in the medium, we analyzed parasite motility as a

403 possible trait linked to invasiveness within spheroids (S6 Fig). We consider a

404 strain (or isolate) as poor motile when more than 20% of the parasites remain at

405 the pellet in this assay. Although the swimming ability of SylvioX10 and CL

406 Brener strains were considerably different and agree with their behavior in

407 spheroids, other strains showed no association between the transmigration

408 inside spheroids and their swimming ability (for example, up to 60% of parasites

409 from 173BB and 401BB -congenital isolates highly migrant in spheroids-

410 remained between the pellet and layer 1).

411

Discussion

413 The infection with the protozoan parasite *Trypanosoma cruzi* evolves from

414 a short acute to a long lasting chronic phase when cardiac, neurological or

415 intestinal disorders become evident [3]. Although the pathology appears only at

416 the chronic phase, the infection of tissues initiates during acute phase and is the

417 consequence of the early dissemination of trypomastigotes. Indeed, *T. cruzi* can

418 disseminate and establish an intracellular infection in any tissue of the

419 mammalian host [5]. To accomplish this, trypomastigotes must migrate and

420 actively cross several biological barriers, from the initial infection site to the

421 target organs of damage, where parasites replicate intracellularly as amastigotes

422 [2]. Murine experimental models of *T. cruzi* infection have helped to understand

423 that some parasite strains present tropism for certain tissues or organs while

424 others are essentially pantropic and can colonize indistinctly any tissue [5,33,34].

18

425 Usually, pantropic strains are more virulent in the murine model. It can be

426 inferred that, since those strains colonize a broader range of tissues, they are

427 also more efficient in the transmigration process. However, how trypomastigotes

428 transmigrate, the mechanisms underlying this process and its significance in the

429 host-parasite interplay are poorly understood.

430 In this work, we employed 3D cultures to mimic the tisular

431 microarchitecture encountered by trypomastigotes in the mammalian host during

432 its *in vivo* life cycle. We studied the process of transmigration and dissemination

433 of the parasites across spheroids for the first time, and demonstrate a link

434 between 3D transmigration and *in vivo* behavior. Strains or isolates that are

435 more virulent *in vivo* (in natural or experimental infections) transmigrated deeper

436 inside spheroids than no virulent strains. In an *in vivo* infection, the ability to

437 transmigrate will favour pathogen dissemination into the host, at the same time

438 that parasites evade the immune system and increase the opportunity to find an

439 adequate microenvironment to settle for the tissular infection [35-38].

440 By employing the 3D spheroid model, we focused on one hand in the

441 ability of *T. cruzi* strains to infect mammalian cells (evaluated by flow cytometry

442 as cells with either internalized or attached parasites). On the other hand, we

443 also examined the invasiveness of trypomastigotes, which means how deep

444 inside the spheroids trypomastigotes are detected. Somehow both events

445 (invasiveness and infection) are linked by the fact that *T. cruzi* strains that were

446 highly migrant were also those that presented higher infection rates, probably

447 because the transmigration was a necessary step to infect the cells located deep

448 inside the spheroids. This fact can also explain why poorly migrant strains

19

449 presented low infection rates in the 3D model, irrespective of their accurate

450 infection rate in conventional 2D monolayer cultures. However, considering the

451 times at which transmigration was analyzed, it is unlikely that transmigration was

452 the result of cellular invasion and replication of parasites. We postulate the

453 transcellular and paracellular transmigration routes as two possible ways for

454 trypomastigotes to reach the deeper layers of spheroids. Even more, we

455 speculate that how *T. cruzi* transmigrates can be also a strain dependent trait

456 and that different strains or isolates can employ differential transmigration

457 strategies. Electronic microscopy images strongly suggest that CL Brener strain

458 goes through spheroids by a paracellular route, without crossing the cells but

459 between cell-cell junctions. Although the biological significance of this

460 transmigration strategy should be carefully studied, we hypothesize that the

461 paracellular route would allow the parasite to internalize into the tissues without

462 disrupting the cellular homeostasis and, therefore, without triggering an

463 inflammatory response. Moreover, a paracellular route would be a faster

464 transmigration mechanism for trypomastigotes to find their target allocation

465 inside tissues, without the need to invade and replicate intracellularly. In line with

466 these results, Coates et al (2013) showed that *T. cruzi* trypomastigotes can

467 cross a monolayer of endothelial cells without cell damage. They suggested that

468 this process might be mediated by the protease cruzipain, which can convert

469 kininogen to bradykinin (involved in endothelial permeability) [7]. The picture of

470 trypomastigotes distribution was very distinctive between CL Brener and

471 SylvioX10 strains, even from the initial steps of interaction with mammalian cells

472 in our 3D model. While CL Brener trypomastigotes are regularly distributed and

473 positioned in between cell-cell junctions on the external layers of the spheroid

20

474   surface, SylvioX10 trypomastigotes are grouped in patches of several parasites

475   stuck over the cells. Previous works with *Trypanosoma brucei* evidenced that

476   trypomastigotes can cross the blood brain barrier both by transcellular and

477   paracellular routes, promoting the expression of ICAM-1 and VCAM-1 [39-41].

478   On the other hand, *T. gondii* employs a paracellular route for tissue

479   transmigration, through the interaction between TgMIC2 and host occludins from

480   TJs and ICAM-1[42,43]. Interference with the transmigration process avoids *in*

481   *vivo* infectivity both in *T. gondii* and *P. falciparum* [44,45]. Interestingly, the loss

482   of genes associated with transmigration in *P. falciparum* did not impair cellular

483   invasion, supporting the idea that tissue invasiveness and cellular infection can

484   be two independent processes [45].

485   Trypomastigote's motility can be understood as its ability to present a

486   directional movement, which in turn could impact on the cellular infection rates.

487   We found a pronounced difference in swimming motility between SylvioX10 (low

488   migrant and low motile) and CL Brener (high migrant and high motile)

489   trypomastigotes. However, analyses of a broader panel of strains demonstrated

490   that transmigration cannot be solely explained by the motile ability of

491   trypomastigotes. Presumably, transmigration depends both on motility and

492   migration of the parasite as well as on its interaction with the surrounding

493   microenvironment. In this sense, Barragan *et al*, (2002) showed that a high

494   migration rate of *T. gondii* is associated with a highly virulent phenotype [46].

495   Indeed, correlation between high virulent strains and congenital toxoplasmosis

496   has also been noted [47,48]. On the other hand, Éva Dóró et al (2019) have very

497   recently evaluated the migration of trypomastigotes of *T. carassii* in an *in vivo*

498   model. This awesome work clearly shows that the movement of parasites inside

21

499 zebrafish occurs through the interstitial space and how its density and

500 compaction determines the direction of trypomastigotes migration [49].

501   During congenital transmission of *T. cruzi* infection, trypomastigotes must

502 cross epithelial and connective tissues that compose the placental barrier to gain

503 access to and infect the fetus. Therefore, transplacental infection is another

504 aspect of *T. cruzi*-host interplay that is associated with parasite transmigration.

505 We have characterized the invasiveness inside spheroids of isolates recently

506 obtained from babies born with congenital Chagas disease. We demonstrated

507 that the congenital isolates were highly invasive into spheroids, in contrast with

508 the isolate obtained from a mother, which after delivered several children never

509 transmitted the infection to her offspring, which showed a low/moderate

510 transmigration ability. *T. cruzi* congenital transmission is the result of a complex

511 interaction between trypomastigotes and the placental barrier [50-52]. Recently,

512 Juiz et al (2017) described a differential placental gene response induced by

513 strains with different tropism and virulence. They reported that a strain that was

514 isolated from a human case of congenital infection (VD) presented higher

515 tropism by the murine placenta than a non-virulent and myotropic strain (K-98)

516 [53]. In our 3D model, K-98 strain showed a low migrant phenotype. Although we

517 did not analyze the transmigration profile of VD strain, all the congenital isolates

518 assayed here were highly migrant.

519   The intratisular migration is key during the development of metastasis

520 and it has been approached in several studies on cancer [54]. Tumoral cells

521 produce and prompt to the secretion of cytokines and proteases that will favour

522 the migration across different biological barriers. Proteases are necessary to

22

523   disrupt cell-cell junctions, extracellular matrix and the basal lamina [55]. Although

524   little is known about the transmigration process in host-pathogen interactions,

525   the secretion of proteases could also be required to disrupt intercellular junctions

526   and extracellular matrix for *T. cruzi* transmigration. However, in our experimental

527   conditions, the invasiveness was not a transferable feature between strains,

528   neither by soluble or secreted factors nor by co-cultivation of invasive and non-

529   invasive trypomastigotes. This observation suggests that unsecreted and strain

530   specific factors are required to transmigrate into the spheroids, while it does not

531   exclude the involvement of proteases and other soluble factors. Differentially-

532   expressed and/or strain specific membrane-associated molecules from

533   trypomastigotes might be targets to be evaluated in the near future.

534   Altogether, our results demonstrated that in a 3D microenvironment each

535   strain presents a characteristic migration pattern and tissular distribution that

536   could be associated to their *in vivo* behavior. Our work also validates the

537   accuracy and utility of the 3D spheroid model to study complex host-parasite

538   interactions. Certainly, the findings presented here could not have been studied

539   with traditional 2D monolayer cultures.

540

Acknowledgements

23

546 Promoción Científica y Tecnológica / Fondo para la Investigación Científica y

547 Tecnológica -ANPCyT/FONCyT- (PICT-2016-0108 to VT and PICT 2017-2644

548 to MER) from Argentina. The funders had no role in study design, data collection

549 and analysis, decision to publish, or preparation of the manuscript.

550

551 References

552 1. OPS OMS | Enfermedad de Chagas. 2015. Available from:

553 http://www.paho.org/hq/index.php?option=com_topics&view=article&id=10

554 &Itemid=40743&lang=es

555 2. Andrade LO, Andrews NW. Opinion: The Trypanosoma cruzi–host-cell

556 interplay: location, invasion, retention. Nat Rev Microbiol. 2005; 3(10):819–

557 23.

558 3. Rassi A, Rassi A, Marin-Neto JA, al. et, al. et, Guillen I de. Chagas

559 disease. Lancet. 2010; 375(9723):1388–402.

560 4. Lewis MD, Francisco AF, Taylor MC, Jayawardhana S, Kelly JM. Host and

561 parasite genetics shape a link between Trypanosoma cruzi infection

562 dynamics and chronic cardiomyopathy. Cell Microbiol 2016; 18(10):1429–

563 43.

564 5. Costa FC, Francisco AF, Jayawardhana S, Calderano SG, Lewis MD,

565 Olmo F, et al. Expanding the toolbox for Trypanosoma cruzi: A parasite line

566 incorporating a bioluminescence-fluorescence dual reporter and

567 streamlined CRISPR/Cas9 functionality for rapid in vivo localisation and

568 phenotyping. PLoS Negl Trop Dis. 2018; 12(4):e0006388.

24

569 6.   Prado CM, Jelicks LA, Weiss LM, Factor SM, Tanowitz HB, Rossi MA. The

570   vasculature in chagas disease. Adv Parasitol. 2011; 76:83–99.

571 7.   Coates BM, Sullivan DP, Makanji MY, Du NY, Olson CL, Muller WA, et al.

572   Endothelial Transmigration by Trypanosoma cruzi. PLoS One. 2013;

573   8(12):e81187.

574 8.   Lewis MD, Fortes Francisco A, Taylor MC, Burrell-Saward H, McLatchie

575   AP, Miles MA, et al. Bioluminescence imaging of chronic Trypanosoma

576   cruzi infections reveals tissue-specific parasite dynamics and heart disease

577   in the absence of locally persistent infection. Cell Microbiol. 2014;

578   16(9):1285–300.

579 9.   Santi-Rocca J, Gironès N, Fresno M. Multi-Parametric Evaluation of

580   Trypanosoma cruzi Infection Outcome in Animal Models. In: Methods in

581   molecular biology (Clifton, NJ). 2019. p. 187–202.

582 10. Shamir ER, Ewald AJ. Three-dimensional organotypic culture: experimental

583   models of mammalian biology and disease. Nat Rev Mol Cell Biol. 2014;

584   15(10):647–64.

585 11. Fennema E, Rivron N, Rouwkema J, van Blitterswijk C, de Boer J.

586   Spheroid culture as a tool for creating 3D complex tissues. Trends

587   Biotechnol. 2013; 31(2):108–15.

588 12. Zanoni M, Piccinini F, Arienti C, Zamagni A, Santi S, Polico R, et al. 3D

589   tumor spheroid models for in vitro therapeutic screening: a systematic

590   approach to enhance the biological relevance of data obtained. Sci Rep.

591   2016; 6(1):19103.

592 13. Baruzzi A, Remelli S, Lorenzetto E, Sega M, Chignola R, Berton G. Sos1
593   Regulates Macrophage Podosome Assembly and Macrophage Invasive
594   Capacity. J Immunol. 2015; 195(10):4900–12.

595 14. Röhland S, Wechselberger A, Spitzweg C, Huss R, Nelson PJ, Harz H.
596   Quantification of in vitro mesenchymal stem cell invasion into tumor
597   spheroids using selective plane illumination microscopy. J Biomed Opt.
598   2015; 20(4):040501.

599 15. Giannattasio A, Weil S, Kloess S, Ansari N, Stelzer EHK, Cerwenka A, et
600   al. Cytotoxicity and infiltration of human NK cells in in vivo-like tumor
601   spheroids. BMC Cancer. 2015; 15(1):351.

602 16. Garzoni LR, Adesse D, Soares MJ, Rossi MID, Borojevic R, Meirelles M de
603   NL de. Fibrosis and Hypertrophy Induced by Trypanosoma cruzi in a
604   Three-Dimensional Cardiomyocyte-Culture System. J Infect Dis. 2008;
605   197(6):906–15.

606 17. M. Ferrão P, M. Nisimura L, C. Moreira O, G. Land M, Pereira MC, de
607   Mendonça-Lima L, et al. Inhibition of TGF-β pathway reverts extracellular
608   matrix remodeling in T. cruzi -infected cardiac spheroids. Exp Cell Res.
609   2018; 362(2):260–7.

610 18. Cosentino RO, Agüero F. A Simple Strain Typing Assay for Trypanosoma
611   cruzi: Discrimination of Major Evolutionary Lineages from a Single
612   Amplification Product. PLoS Negl Trop Dis. 2012; 6(7):e1777.

613 19. Bernabó G, Levy G, Ziliani M, Caeiro LD, Sánchez DO, Tekiel V. TcTASV-
614   C, a Protein Family in Trypanosoma cruzi that Is Predominantly
615   Trypomastigote-Stage Specific and Secreted to the Medium. PLoS One.

616   2013; 8(7):e71192.

617 20. Rodríguez ME, Rizzi M, Caeiro L, Masip Y, Sánchez DO, Tekiel V.

618   Transmigration of Trypanosoma cruzi Trypomastigotes through 3D

619   Spheroids Mimicking Host Tissues. In: Methods in molecular biology

620   (Clifton, NJ). 2019. p. 165–77.

621 21. Caeiro LD, Alba-Soto CD, Rizzi M, Solana ME, Rodriguez G, Chidichimo

622   AM, et al. The protein family TcTASV-C is a novel Trypanosoma cruzi

623   virulence factor secreted in extracellular vesicles by trypomastigotes and

624   highly expressed in bloodstream forms. PLoS Negl Trop Dis. 2018;

625   12(5):e0006475.

626 22. Gerber PP, Cabrini M, Jancic C, Paoletti L, Banchio C, von Bilderling C, et

627   al. Rab27a controls HIV-1 assembly by regulating plasma membrane levels

628   of phosphatidylinositol 4,5-bisphosphate. J Cell Biol. 2015; 209(3):435–52.

629 23. Carlsson J, Yuhas JM. Liquid-overlay culture of cellular spheroids. Recent

630   Results Cancer Res. 1984; 95:1–23.

631 24. Miller SA, Dykes DD, Polesky HF. A simple salting out procedure for

632   extracting DNA from human nucleated cells. Nucleic Acids Res. 1988;

633   16(3):1215.

634 25. Campo VA. Comparative effects of histone deacetylases inhibitors and

635   resveratrol on Trypanosoma cruzi replication, differentiation, infectivity and

636   gene expression. Int J Parasitol Drugs drug Resist. 2017; 7(1):23–33.

637 26. Ramakers C, Ruijter JM, Deprez RHL, Moorman AF. Assumption-free

638   analysis of quantitative real-time polymerase chain reaction (PCR) data.

639   Neurosci Lett. 2003; 339(1):62–6.

640   27.   Schneider CA, Rasband WS, Eliceiri KW. NIH Image to ImageJ: 25 years

641   of image analysis. Nat Methods. 2012; 9(7):671–5.

642   28.   Zingales B, Miles MA, Campbell DA, Tibayrenc M, Macedo AM, Teixeira

643   MMG, et al. The revised Trypanosoma cruzi subspecific nomenclature:

644   Rationale, epidemiological relevance and research applications. Infect

645   Genet Evol. 2012; 12(2):240–53.

646   29.   Marinho CRF, Nuñez-Apaza LN, Bortoluci KR, Bombeiro AL, Bucci DZ,

647   Grisotto MG, et al. Infection by the Sylvio X10/4 clone of Trypanosoma

648   cruzi: relevance of a low-virulence model of Chagas' disease. Microbes

649   Infect. 2009; 11(13):1037–45.

650   30.   Marinho CRF, Nuñez-Apaza LN, Martins-Santos R, Bastos KRB, Bombeiro

651   AL, Bucci DZ, et al. IFN-gamma, But Not Nitric Oxide or Specific IgG, is

652   Essential for the In vivo Control of Low-virulence Sylvio X10/4

653   Trypanosoma cruzi Parasites. Scand J Immunol. 2007; 66(2–3):297–308.

654   31.   Belew AT, Junqueira C, Rodrigues-Luiz GF, Valente BM, Oliveira AER,

655   Polidoro RB, et al. Comparative transcriptome profiling of virulent and non-

656   virulent Trypanosoma cruzi underlines the role of surface proteins during

657   infection. PLoS Pathog. 2017; 13(12):e1006767.

658   32.   Volta BJ, Bustos PL, Cardoni RL, De Rissio AM, Laucella SA, Bua J.

659   Serum Cytokines as Biomarkers of Early Trypanosoma cruzi infection by

660   Congenital Exposure. J Immunol. 2016; 196(11):4596–602.

661   33.   Santi-Rocca J, Gironès N, Fresno M. Multi-Parametric Evaluation of

28

662   Trypanosoma cruzi Infection Outcome in Animal Models. 2019. p. 187–202.

663   34.   Lewis MD, Francisco AF, Taylor MC, Kelly JM. A New Experimental Model

664   for Assessing Drug Efficacy against Trypanosoma cruzi Infection Based on

665   Highly Sensitive In Vivo Imaging. J Biomol Screen. 2015; 20(1):36–43.

666   35.   Harker KS, Ueno N, Lodoen MB. Toxoplasma gondii dissemination: a

667   parasite's journey through the infected host. Parasite Immunol. 2015;

668   37(3):141–9.

669   36.   Kumar H, Tolia NH. Getting in: The structural biology of malaria invasion.

670   PLOS Pathog. 2019; 15(9):e1007943.

671   37.   Drewry LL, Sibley LD. The hitchhiker's guide to parasite dissemination. Cell

672   Microbiol. 2019; e13070.

673   38.   Lambert H, Barragan A. Modelling parasite dissemination: host cell

674   subversion and immune evasion by Toxoplasma gondii. Cell Microbiol.

675   2010 Mar; 12(3):292–300.

676   39.   Mulenga C, Mhlanga JD, Kristensson K, Robertson B. Trypanosoma brucei

677   brucei crosses the blood-brain barrier while tight junction proteins are

678   preserved in a rat chronic disease model. Neuropathol Appl Neurobiol.

679   2001; 27(1):77–85.

680   40.   Grab DJ, Nikolskaia O, Kim Y V., Lonsdale-Eccles JD, Ito S, Hara T, et al.

681   African trypanosome interactions with an in vitro model of the human blood-

682   brain barrier. J Parasitol. 2004; 90(5):970–9.

683   41.   Nikolskaia O V., de A Lima APC, Kim Y V, Lonsdale-Eccles JD, Fukuma T,

684   Scharfstein J, et al. Blood-brain barrier traversal by African trypanosomes

29

685   requires calcium signaling induced by parasite cysteine protease. J Clin
686   Invest. 2006; 116(10):2739–47.

687 42. Weight CM, Jones EJ, Horn N, Wellner N, Carding SR. Elucidating
688   pathways of Toxoplasma gondii invasion in the gastrointestinal tract:
689   involvement of the tight junction protein occludin. Microbes Infect. 2015;
690   17(10):698–709.

691 43. Barragan A, Brossier F, Sibley LD. Transepithelial migration of Toxoplasma
692   gondii involves an interaction of intercellular adhesion molecule 1 (ICAM-1)
693   with the parasite adhesin MIC2. Cell Microbiol. 2005; 7(4):561–8.

694 44. Huynh M-H, Carruthers VB. Toxoplasma MIC2 Is a Major Determinant of
695   Invasion and Virulence. PLoS Pathog. 2006; 2(8):e84.

696 45. Yang ASP, O'Neill MT, Jennison C, Lopaticki S, Allison CC, Armistead JS,
697   et al. Cell Traversal Activity Is Important for Plasmodium falciparum Liver
698   Infection in Humanized Mice. Cell Rep. 2017; 18(13):3105–16.

699 46. Barragan A, Sibley LD. Transepithelial migration of Toxoplasma gondii is
700   linked to parasite motility and virulence. J Exp Med. 2002 Jun
701   17;195(12):1625–33.

702 47. Howe DK, Sibley LD. Toxoplasma gondii Comprises Three Clonal
703   Lineages: Correlation of Parasite Genotype with Human Disease. J Infect
704   Dis. 1995; 172(6):1561–6.

705 48. Fuentes I, Rubio JM, Ramirez C, Alvar J. Genotypic Characterization of
706   Toxoplasma gondii Strains Associated with Human Toxoplasmosis in
707   Spain: Direct Analysis from Clinical Samples. J Clin Microbiol. 2001;

30

708   39(4):1566–70.

709 49. Dóró É, Jacobs SH, Hammond FR, Schipper H, Pieters RP, Carrington M,

710   et al. Visualizing trypanosomes in a vertebrate host reveals novel

711   swimming behaviours, adaptations and attachment mechanisms. Elife.

712   2019; 8. e48388.

713 50. Castillo C, Carrillo I, Libisch G, Juiz N, Schijman A, Robello C, et al. Host-

714   parasite interaction: changes in human placental gene expression induced

715   by Trypanosoma cruzi. Parasit Vectors. 2018;11(1):479.

716 51. Juiz NA, Torrejón I, Burgos M, Torres AMF, Duffy T, Cayo NM, et al.

717   Alterations in Placental Gene Expression of Pregnant Women with Chronic

718   Chagas Disease. Am J Pathol. 2018; 188(6):1345–53.

719 52. Bustos PL, Milduberger N, Volta BJ, Perrone AE, Laucella SA, Bua J.

720   Trypanosoma cruzi Infection at the Maternal-Fetal Interface: Implications of

721   Parasite Load in the Congenital Transmission and Challenges in the

722   Diagnosis of Infected Newborns. Front Microbiol. 2019; 10:1250.

723 53. Juiz NA, Solana ME, Acevedo GR, Benatar AF, Ramirez JC, da Costa PA,

724   et al. Different genotypes of Trypanosoma cruzi prod1. Juiz NA, Solana

725   ME, Acevedo GR, Benatar AF, Ramirez JC, da Costa PA, et al. Different

726   genotypes of Trypanosoma cruzi produce distinctive placental environment

727   genetic response in chronic experimental infecti. PLoS Negl Trop Dis.

728   2017; 11(3):e0005436.

729 54. Stuelten CH, Parent CA, Montell DJ. Cell motility in cancer invasion and

730   metastasis: insights from simple model organisms. Nat Rev Cancer. 2018;

731   18(5):296–312.

31

732   55.   Wolf K, Friedl P. Extracellular matrix determinants of proteolytic and non-

733   proteolytic cell migration. Trends Cell Biol. 2011; 21(12):736–44.

734

735

Figure captions

Fig 1. Model setup.

738   (A) *Trypanosoma cruzi* SylvioX10 (DTU TcI) and CL Brener (DTU TcVI)

739   trypomastigotes were labelled with CFSE: fluorescent images (left panel) and

740   quantification by flow cytometry (right panel). Black histograms: non-labelled

741   parasites; green histograms: CFSE labelled parasites. NS: Negative Staining.

742   (B) Spheroid of HeLaR2 cells at 72 h post seeding. Scale bar = 100 µm.

743

Fig 2. Differential ability of SylvioX10 and CL Brener trypomastigotes to infect 2D-monolayer vs 3D-spheroid cultures.

746   HeLaR2 (grown as monolayers or as spheroids, see Material and Methods

747   section) were incubated with 10 m.o.i. of CFSE-labelled CL Brener or SylvioX10

748   trypomastigotes or non-infected (control). (A, B) At 24 h post infection, cells

749   were trypsinized and the rate of infected HeLaR2 cells (either with internalized or

750   attached parasites) was determined by flow cytometry. (C) Quantification of

751   three independent experiments carried out as described for A and B. (D)

752   Quantification of the total parasite cargo inside spheroids, which includes both

753   cell-associated parasites and free parasites inside spheroids from three

754   independent experiments. At 24 h post infection either intact spheroids or the

755 whole content of the well (intact spheroids plus culture media with non-

756 internalized parasites) were harvested and total DNA purified. Parasite content

757 was estimated on the basis of qPCR of a single copy *T. cruzi* gene (*PCD6*,

758 TriTryp gene ID: TcCLB.507099.50). Percentage of *T. cruzi* DNA inside

759 spheroids respect to total *T. cruz*i DNA in the well was calculated. (E) Free

760 parasites inside spheroids infected with CL Brener or SylviX10, at 24 h p.i.

761 Representative confocal images of disaggregated spheroids, white arrows:

762 magnified cells; white asterisks: free parasites. (F) Quantification of free

763 parasites released from disaggregated spheroids. Data expressed as number of

764 free-parasites for each 100 HeLaR2 cells. Graphs represent the mean ± SD of

765 three independent experiments *t test,* *p<0.05, **p<0.01, ***p<0.001.

766

767 **Fig 3. Differential dissemination pattern within spheroids of different**

768 **strains of *T. cruzi*.**

769 (A and B)**.** 3D reconstruction of HeLaR2 spheroids infected with CFSE-

770 SylvioX10 or CFSE-CL Brener trypomastigotes. Z-stack images were obtained

771 by confocal microscopy. The distribution on the surface (X-Y left image), the

772 side plane (Z-Y middle image) and inside the spheroid (Y-X right image,

773 transversal view) are shown. Green: CFSE-trypomastigotes. Red: LifeAct-RFP

774 of HeLa cells. (C and D) Representative images of three confocal planes

775 obtained at 10, 30 and 50 μm in depth on the z axis (40x objective). The detailed

776 distribution pattern of parasites is observed -green fluorescence-. Scale bar: 100

777 μm.

778

33

779 **Fig 4. Differential host cell-parasite interaction pattern of different strains**

780 **of *T. cruzi* on the spheroid surface.**

781 Spheroids were cultured with CFSE-SylvioX10 or CFSE-CL Brener. (A) Cell-

782 parasite interaction on the surface of infected spheroids after 24 h of infection.

783 SEM microscopy showing the whole surface of infected spheroids (images a and

784 d) or detailed cell-parasite interactions (b-c for SylvioX10 and e-f for CL Brener)

785 are shown. White arrows show groups of parasites on the surface of SylvioX10

786 infected spheroids. White asterisks show CL Brener parasites located in the site

787 of cell cell-cell contact. Scale bar for a and d: 100 μm; b and c: 10 μm; d: 100

788 μm; e: 10 μm: f: 5 μm. (B) Confocal microscopy capturing cell infection at 10 μm

789 of infected spheroids with 60x objective. The distribution pattern of parasites on

790 the surface of infected spheroids is observed in a and d images for SylvioX10

791 and CL Brener, respectively. Blue arrows show magnified insets (b-c for

792 SylvioX10 and e-f for CL Brener). Yellow asterisks show multi-infected cells.

793 White asterisks show cell-cell contact associated parasites. Scale bar = 15 μm.

794 (C) Multi-infected cell on the surface of SylvioX10 infected spheroids was

795 reconstructed in 3D. Multiple intracellular amastigotes can be observed. (D)

796 Spheroids of HeLaR2 cells were incubated with CFSE-CL Brener

797 trypomastigotes for 1h and then photographed by confocal microscopy. CFSE-

798 trypomastigotes in the paracellular space both in fluorescence images (a) as well

799 as in bright light (b) are shown. Scale bar 15 μm.

800

801 **Fig 5. Invasiveness within spheroid is an intrinsic feature of each strain,**

802 **not complemented in trans.**

34

803 Spheroids of HeLaR2 cells were incubated with CFSE-CL Brener, CTFR-CL

804 Brener, CFSE-SylvioX10 or CTFR-SylvioX10 or simultaneously co-incubated

805 with both strains labelled with different dyes. (A) Representatives images of

806 three confocal planes obtained at 10, 30 and 50 μm in depth -on the z axis- with

807 a 40x objective. Cyan: CTFR-SylvioX10; green: CFSE-CL Brener; red: HeLaR2

808 cells. Magnified insets (a-d) are shown in the right panels. Scale bar = 100 μm.

809 (B) The same assay as described in A but spheroids were disaggregated and

810 cells with either attached or internalized parasites were quantified by flow

811 cytometry. Infections with one (mono-infections) or both strains simultaneously

812 (co-infections) were carried out also with interchanged dyes. The percentage of

813 infected cells was significantly different between SylvioX10 and CL Brener

814 parasites in all conditions tested. On the other hand, no differences in the

815 infection rate for each strain, both with the use of different staining dyes, as well

816 as, during the mono infections versus the co-infections were observed. Graphs

817 represent the mean ± SD of three independent experiments. Data were analyzed

818 by ane-way ANOVA followed by Bonferroni's multiple comparison test.

819

820 **Fig 6. The capacity of dissemination is linked to virulence.**

821 Spheroids of HeLaR2 cells were incubated with k98, Dm28c, Y or RA strains for

822 24 h. Three confocal planes were obtained at 10, 30 and 50 μm in depth -on the

823 z axis- with 40x objective. The detailed distribution pattern of parasites is

824 observed. 3D-reconstruction is shown in lower panels. Green: CFSE labeled

825 parasites. Red: LifeAct-RFP. Scale bar = 100 μm.

826

35

Fig 7. Congenital trypomastigotes are more invasive and infective than non-congenital parasites.

Spheroids of HeLaR2 cells were incubated with 733MM, 173BB, 401BB or 748BB recent clinical isolates for 24 h. (A) Confocal planes were obtained at 10, 30 and 50 μm in depth -on the z axis- with 40x objective. The detailed distribution pattern of parasites is observed. Sacle bar = 100 μm. (B) Three-D-reconstruction of infected spheroids with each strain is shown. Green: CFSE labeled parasites. Red: LifeAct-RFP. (C) Percentage of infected HeLaR2 cells to compare infectivity of non-congenial vs congenital isolated. Pink and blue bars show SylvioX10 and CL Brener % of infection, respectively, as comparison points. Graphs represent the mean ± SD of three independent experiments.

Supporting information captions

S1 Fig. Genotyping of *T. cruzi* strains and isolates (according to Cossentino et al, 2012).

(A) TcSC5D amplification product was digested with SphI/HpaI restriction enzymes and fragments resolved in 2% agarose gels. Fragment length polymorphism defined lineages TcI for SylvioX10, K98, 733MM and 173BB; TcII for Y; TcV/VI for CL Brener, RA, 401BB and 748BB. (B) The digestion of TcMK product with XhoI allows to distinguish between DTUs TcV (401BB and 748BB) and TcVI (CL Brener and RA).

S2 Fig. The 3D culture model.

36

851   (A) Monolayer of HeLa cells stably expressing LifeAct-RFP (HeLaR2), generated

852   by lentiviral infection of the parental HeLa cells. (B) Spheroids formation by liquid

853   overlay. After 24 h, spheroids are irregular aggregates of cells. From 72 h after

854   culturing, spheroids seem to be compact aggregate of cells with well delimited

855   borders.

856

857   **S3 Fig. Infection of 2D-monolayer and spheroids at m.o.i. 1, with strains CL**

858   **Brener and Sylvio.**

859   HeLaR2 cells were incubated with CFSE-labelled trypomastigotes for 24 h and

860   then monolayers or spheroid cultures fixed. (A) the Infected cells were

861   determined by flow cytometry, which detects both attached and internalized

862   parasites. (B) Quantification of 3 independent experiments, carried out as

863   described for A**.** (C, D) Spheroids were disaggregated and released parasites

864   (free parasites inside spheroids) were visualized by fluorescence microscopy

865   and quantified. * *t test* <0.05.

866

867   **S4 Fig. Dissemination pattern within spheroids of CL Brener after 1 h of**

868   **infection.**

869   Spheroids incubated with 10 m.o.i. of CFSE-CL Brener parasites for 1h were

870   fixed and confocal planes were obtained at 10, 30 and 50 µm in depth -on the z

871   axis- with 40x objective. Representative images of the invasiveness of CL

872   Brener parasites -green fluorescence- that were detected even at 50 µm in depth

873   within the spheroids. Scale bar = 100 µm.

874

37

875 **S5 Fig. Invasiveness within spheroid is not mediated by soluble factors.**

876 (A) spheroids were incubated with CFSE-CL Brener (left) or CFSE-SylvioX10

877 (right) trypomastigotes for 24 h along with control media, or conditioned media

878 (CM) from either SylvioX10 or CL Brener trypomastigotes. Then, spheroids were

879 fixed and confocal images were taken at 10, 30 and 50 µm in depth from

880 spheroid surface. (B) Spheroids incubated with CL Brener or SylvioX10

881 trypomastigotes in presence of control media or conditioned media were

882 disaggregated with trypsin and % of infected cells was measured by flow

883 cytometry.

884

885 **S6 Fig. The free motility *in vitro* is not associated with invasion inside**

886 **spheroids.** Trypomastigotes were pelleted in round bottom tubes and then

887 incubated for 2 h at 37ºC in medium to allow free-swimming (Left image).

888 Aliquots of 1 ml (layer 1 to 5) of the medium from top to bottom were carefully

889 collected and quantification of the % of parasites in each layer and pellet was

890 carried out by microscopy, on Neubauer chamber (graph). Isolates / strains are

891 classified in two groups: those that presented low motility [>40 % of

892 trypomastigotes in the pellet after 2 h] and those with high motility [<20% of

893 parasites in the pellet] and trypomastigotes were homogeneously distributed

894 among all layers]. As a reference, the low migran strains (into spheroids) are in

895 pink and the high migrants are in sky blue. pasa a suplementaria

896

897 **S1 and S2 movies.**

898 HeLaR2 spheroid infected with CFSE-SylvioX10 (video1) or CFSE-CL Brener

38

899 (video 2); 3D reconstruction. Z-stack images were obtained by confocal

900 microscopy using 10x objective. The videos were realized by using ImageJ

901 software -3D viewer plugin-. Half of an infected spheroid rotating on the Y axis is

902 shown. Green: CFSE-parasites. Red: LifeAct-RFP of HeLa cells.

903

904 **S3 movie.**

905 3D reconstruction of a single HeLaR2 cell on the surface of a SylvioX10-infected

906 spheroid.   Z-stack images were obtained by confocal microscopy using 60x

907 objective. The video was realized by using ImageJ software -3D viewer plugin-.

908 Multiple amastigotes within a single cell are shown. Green: CFSE-parasites.

909 Red: LifeAct-RFP of HeLa cells.

910

911 **S4 movie.**

912 3D reconstruction of a single CL Brener trypomastigote located inside the

913 spheroid (≈30 μm deep) after 1 h of incubation. Z-stack images were obtained

914 by confocal microscopy using 60x objective. The video was realized by using

915 ImageJ software -3D viewer plugin-. The paracellular location of the

916 trypomastigote is shown. Green: CFSE-parasites. Red: LifeAct-RFP of HeLa

917 cells.

918

919 **S5 movie.**

920 The video shows the scanning of the first 20-30 μm (from the surface to the

39

921   center) of a CL Brener-infected spheroid after 1 h of incubation. Z-stack images

922   were obtained by confocal microscopy using 60x objective. The video was

923   realized by using ImageJ software. White arrow shows the paracellular located

924   trypomastigote. Green: CFSE-trypomastigotes. Gray: HeLa cells.

925

926   **S6 movie**

927   3D reconstruction of a single intracellular CL Brener trypomastigote located

928   inside the spheroid (20-30 µm deep) after 1 h of incubation. Z-stack images were

929   obtained by confocal microscopy using 60x objective. The video was realized by

930   using ImageJ software -3D viewer plugin-. Green: CFSE-trypomastigotes. Red:

931   LifeAct-RFP of HeLa cells.

932

933   **S7 and S8 movies**

934   3D reconstruction of a HeLaR2 spheroid infected with CFSE-Y trypomastigotes

935   (video 7) or CFSE-RA trypomastigotes (video 8). Z-stack images were obtained

936   by confocal microscopy using 10x objective. The video was realized by using

937   ImageJ software -3D viewer plugin-. A half of an infected spheroids rotating on

938   the Y axis shown. Green: CFSE-parasites. Red: LifeAct-RFP of HeLa cells.

939

940

941

942

40

943

944

945

946

947

948
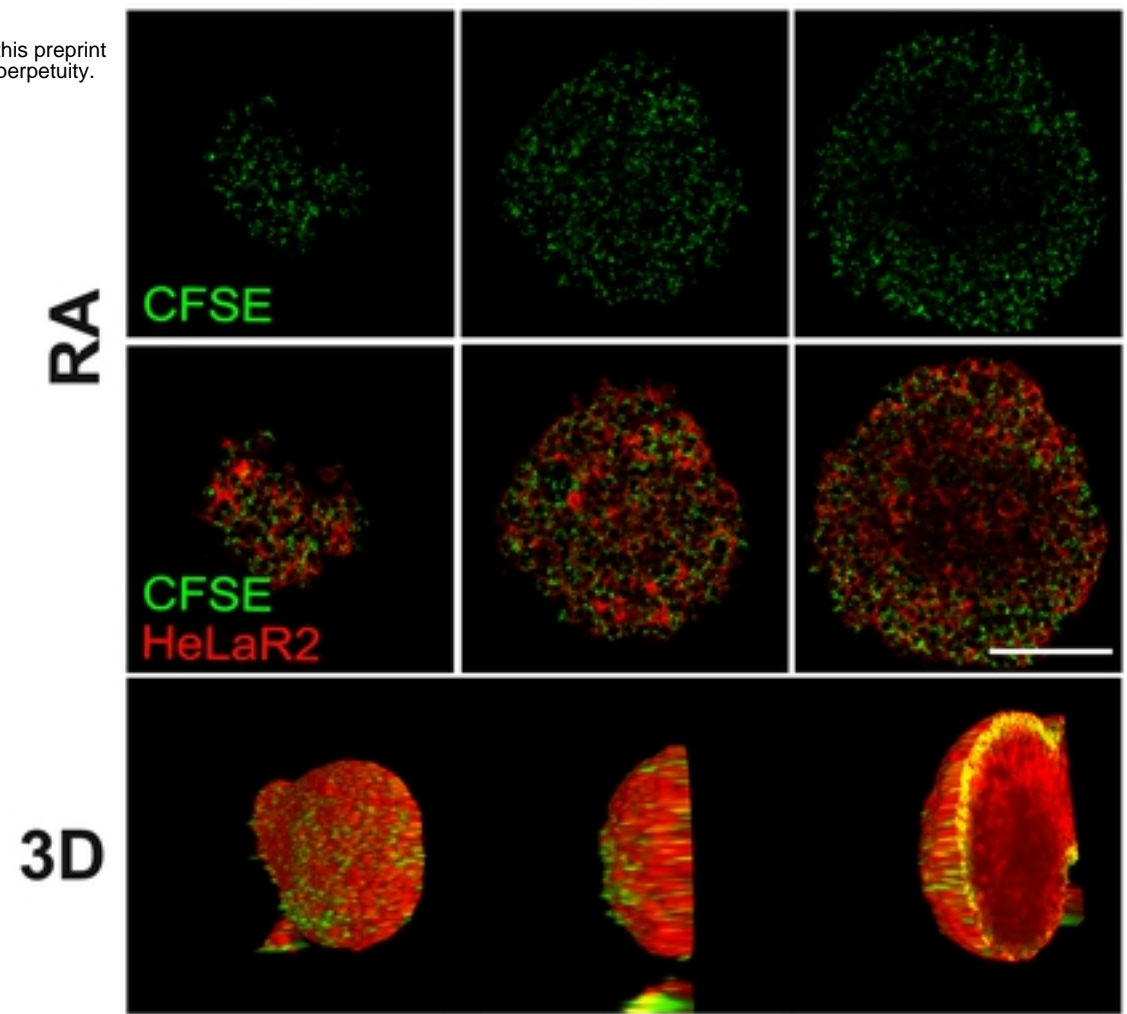
41

A

Depth in the Z-axis

| 10 μm | 30 μm | 50 μm |

199-733MM
CFSE
CFSE HeLaR2

193-173BB
CFSE
CFSE HeLaR2

Depth in the Z-axis

| 10 μm | 30 μm | 50 μm |

186-401BB
CFSE
CFSE HeLaR2

185-748BB
CFSE
CFSE HeLaR2

B

3D reconstruction
CFSE-parasites / HeLaR2 spheroids

Y-X   Y-Z   X-Y

199-733MM

193-173BB

186-401BB

185-748BB

C

% of infected (CFSE+) HeLaR2 cells

N I SylvioX 10 733MM CL Brener 173BB 401BB 748BB

Non-congenital   Congenital

Fig 7
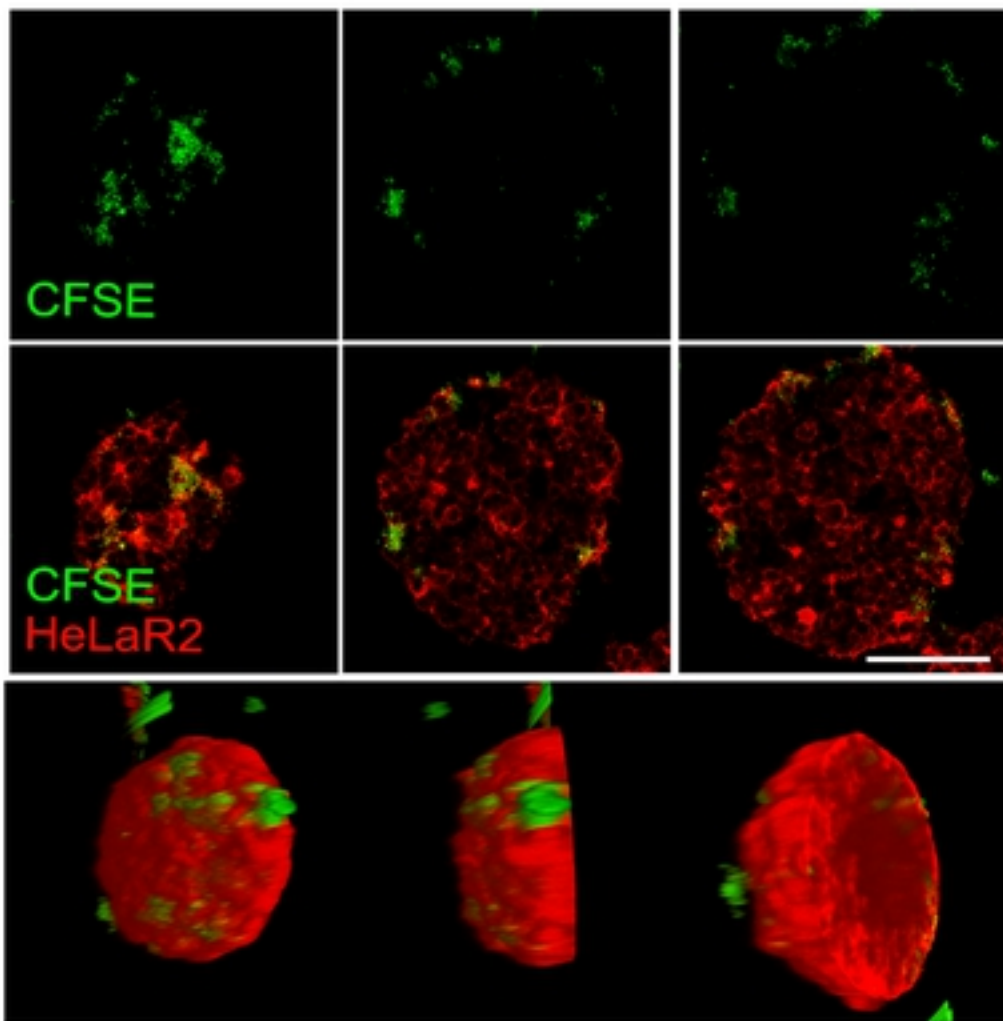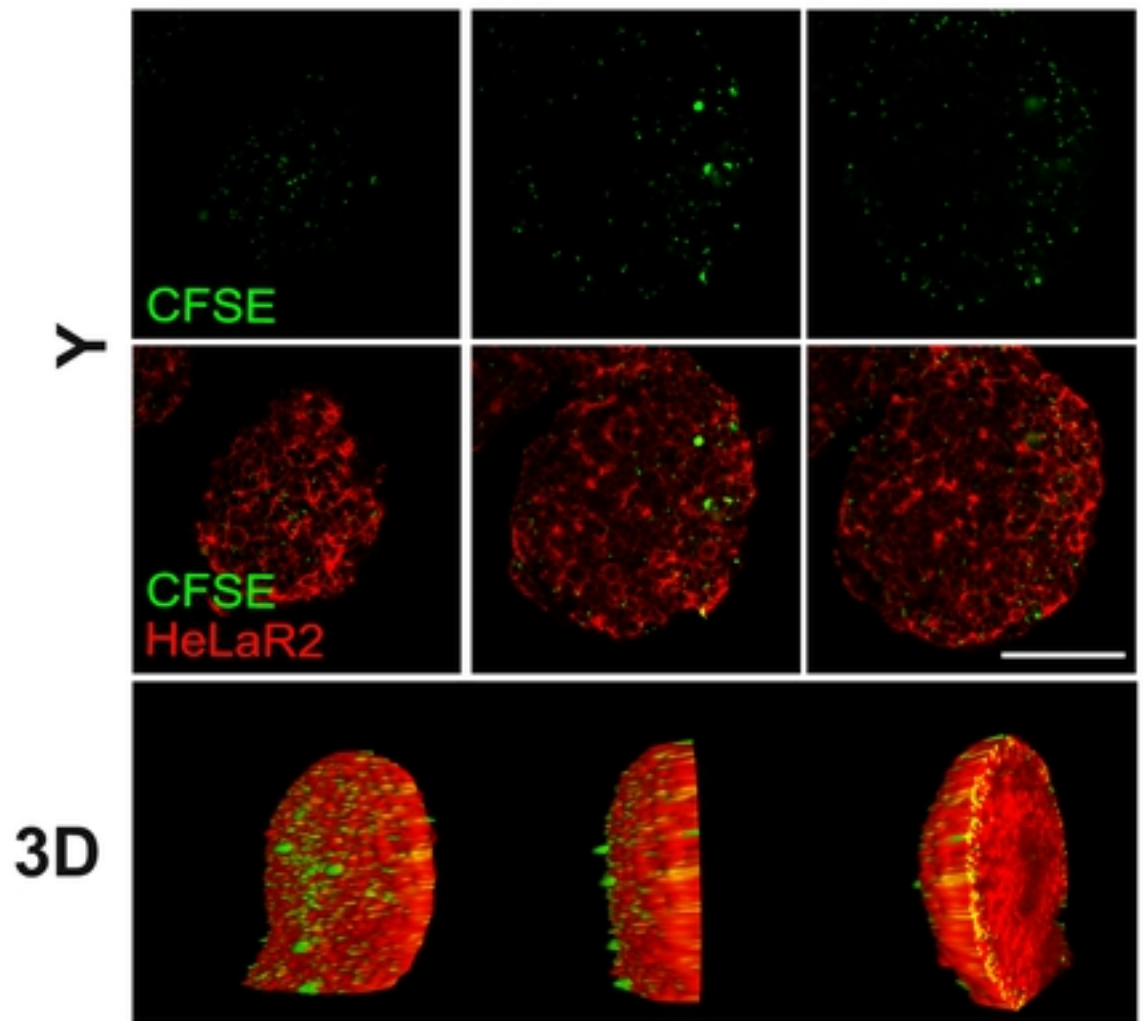
Fig 6

A

Depth in the Z-axis

B

Fig 5

A

SylvioX10: a, b, c

CL Brenr: d, e, f

B Insets

SylvioX10: a, b, c

HeLaR2
SylvioX10 CFSE

CL Brenr: d, e, f

HeLaR2
CL Brener CFSE

C

SylvioX10 infected HeLaR2 cell

HeLaR2
SylvioX10 CFSE

X-Y   Y-Z
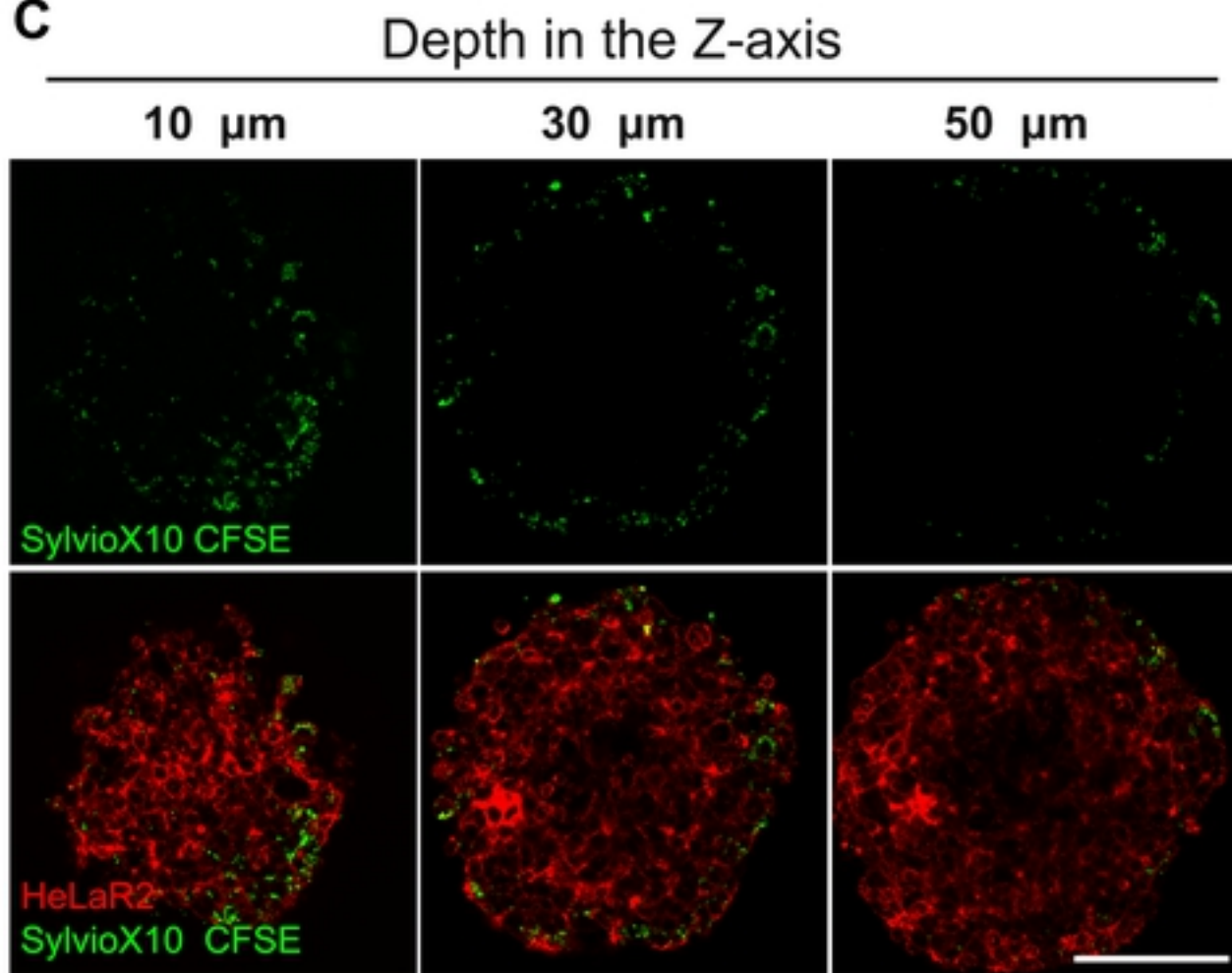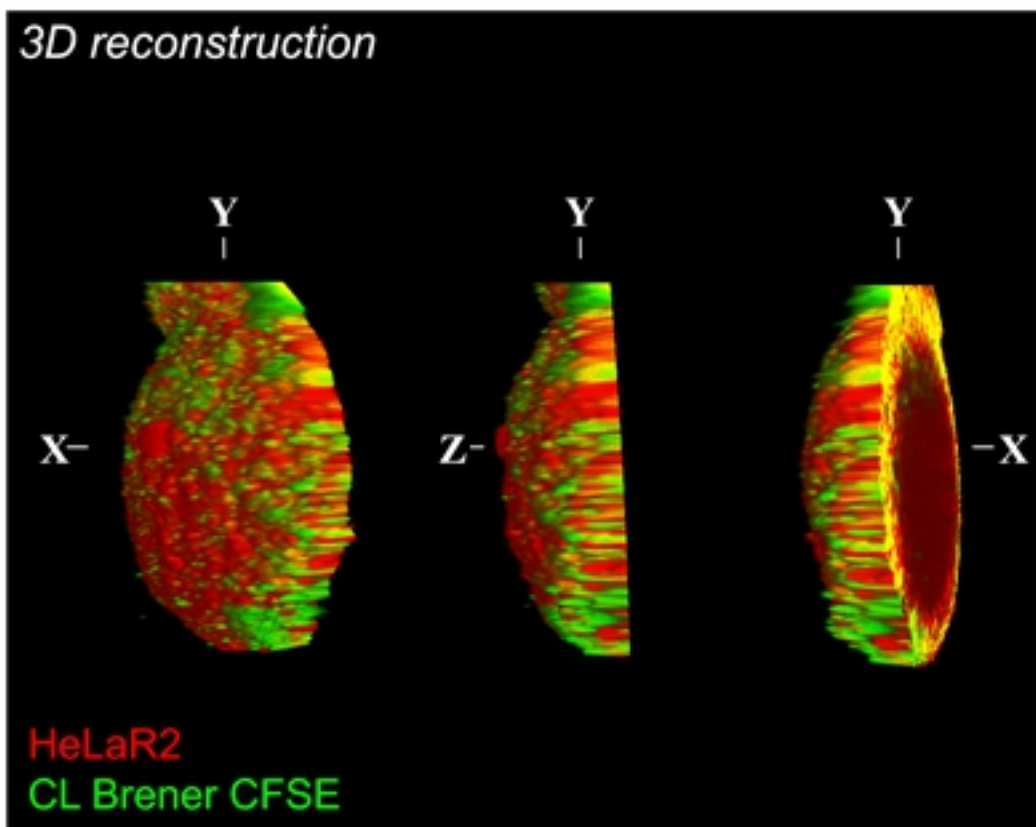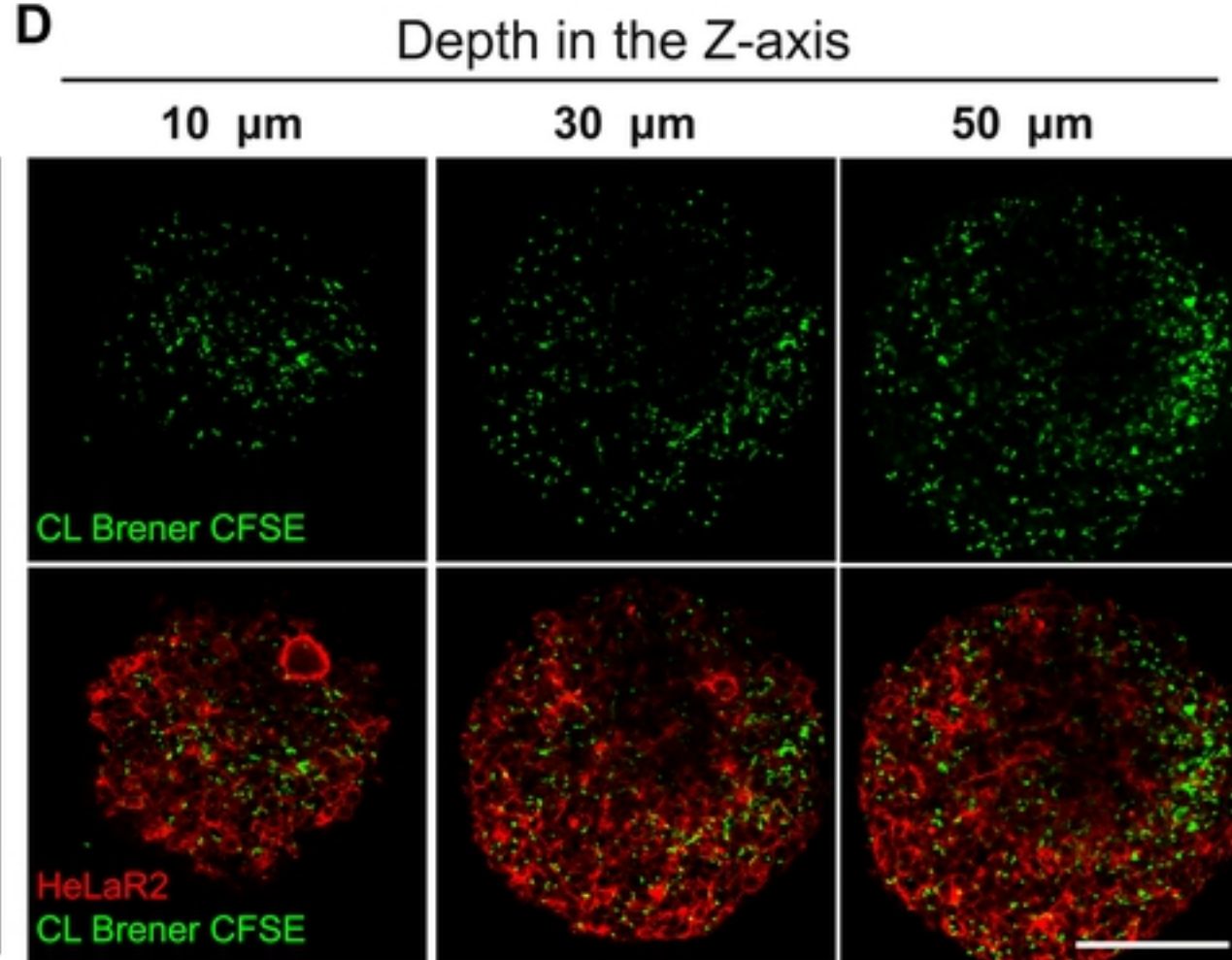
D CL Brener infected spheroids

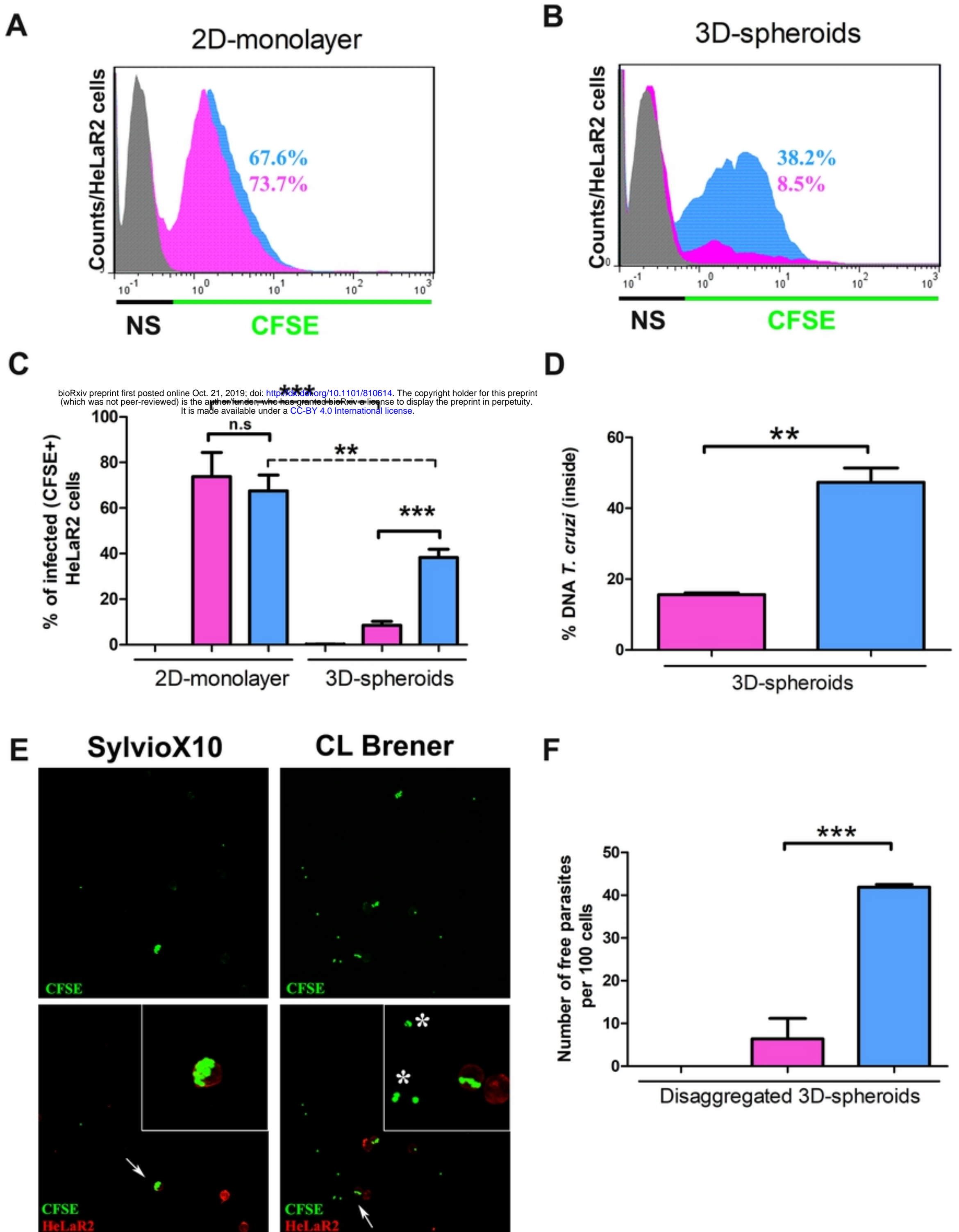Paracellular: a, b
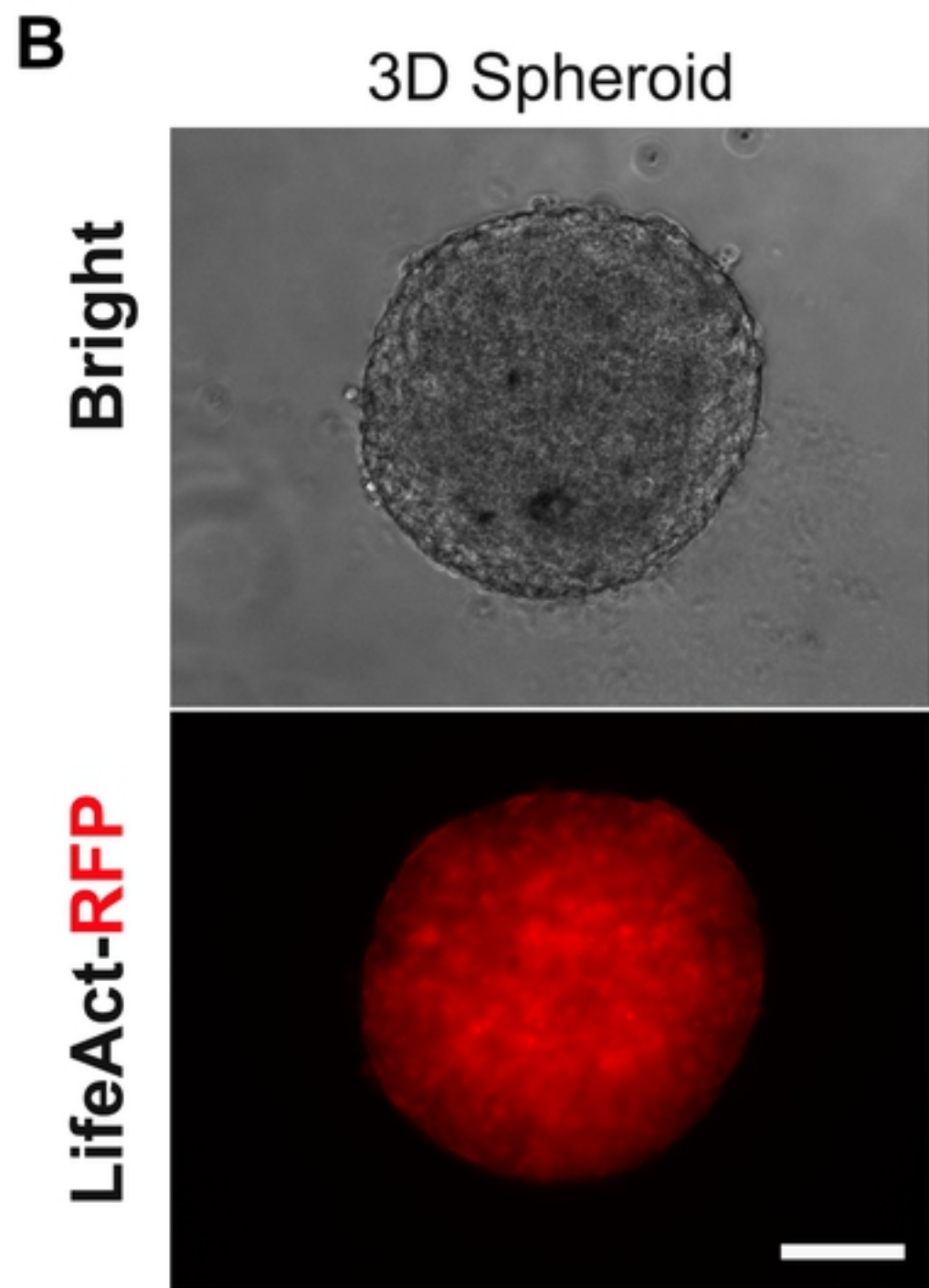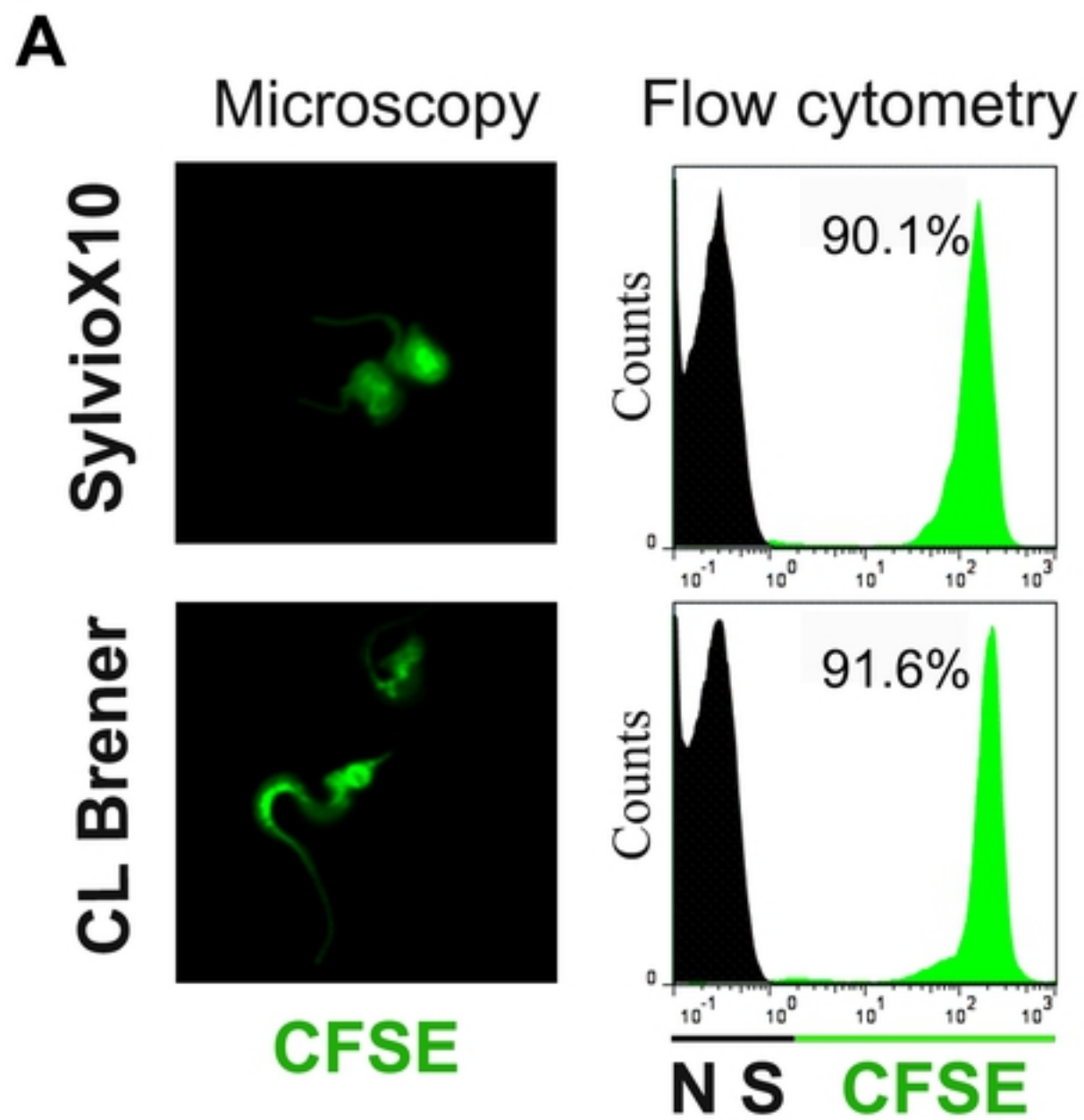
HeLaR2
CL Brener CFSE

Fig 4

Fig 3

Non-infected   SylvioX10   CL Brener

A 2D-monolayer

B 3D-spheroids

C

D

E SylvioX10   CL Brener

F

Fig 2

A

Microscopy   Flow cytometry

SylvioX10

CFSE

90.1%

Counts

10^{-1} 10^0 10^1 10^2 10^3

CL Brener

91.6%

Counts

10^{-1} 10^0 10^1 10^2 10^3

CFSE

N S   CFSE

B   3D Spheroid

Bright

LifeAct-RFP

Fig 1